Effect of high temperature on structural behaviour of metal-to-metal seal in a pressure relief valve

Ali Anwar*, Yevgen Gorash, William Dempster, Robert Hamilton, David Nash
Weir Advanced Research Centre, University of Strathclyde, UK

ABSTRACT

This paper presents a numerical study involving the deformation of contact faces for a metal-to-metal seal in a typical pressure relief valve. The valve geometry is simplified to an axisymmetric problem, which comprises a simple geometry consisting of only three components: A cylindrical nozzle; which is in contact with a disc (representing the valve seat on top); which is preloaded by a compressed linear spring. The nozzle-disk pair is made of the austenitic stainless steel AISI type 316N(L) steel, which is typically used for power plant components. In a previous study, the macro-micro interaction of Fluid Pressure Penetration (FPP) was carried out in an iterative manual procedure at a temperature of 20°C. This procedure is now automated and implemented through an APDL script, which adjusts the spring force according to the current depth of FPP at a macroscale to maintain a consistent seal at elevated temperatures. Based upon the obtained results, specific suggestions to improve the leak tightness of the metal-to-metal seals at elevated temperatures are formulated.

1   INTRODUCTION

As the operating pressure within a valve reaches the set pressure, the sensitivity of the valve opening prior to reaching an equilibrium (set pressure=operating pressure) increases since the leakage through the contacting gap increases. Commonly, metal-to-metal contact Pressure Relief Valves (PRV) are capable of leaking when in a closed state. Standards such as BS6759-3:1984 [1], ASME / ANSI PTC 25.3 [2] and API standard 527 [3] are used to account for and quantify the leakage within safe specifications.

The service characteristics of a valve range from fluid type, fluid characteristics, pressure, temperature, chemical resistance and finally operational and maintenance requirements [4]. Appropriate valve selection is dependent on complete knowledge of the required function and the service characteristics.

This paper focuses on the structural behaviour of the metal-to-metal contact seal in a PRV when the material, AISI type 316N(L) steel, behaves and reacts as it would when exposed to a higher temperature. In this case the temperature of interest is 538°C (maximum operating temperature for the investigated valve) and the fluid being a gas i.e. air. The maximum operating pressure supported by the valve in question is 18.6 MPa.

To study these specific effects of temperature and pressure a finite element analysis is undertaken using ANSYS Parametric Design Language (APDL) script to account for Fluid Pressure Penetration (FPP) through the contact gap. This APDL script allows for pressure between the contact gap to be accounted for sufficiently and automatically adjusting the force retraining the valve from opening. Ultimately this allows for a cyclic analysis of the valve opening and closing with FPP accounted for.

This research builds upon the work conducted by Gorash et al. [5], 'Modelling of metal-to-metal seals in a pressure relief valve using advanced FE-analysis'. In particular, this research advances in the: structural model by analysis conducted at an elevated temperature; with a more accurate material model to consider viscoplastic deformation at high temperature; by creating an APDL script to automatically account for the FPP migration; and adjustment of the spring force to maintain the desire set pressure.

2   SEAT CONTACT CONFIGURATION

The PRV is simplified into three 2D axisymmetric basic parts: a cylindrical nozzle; which is in contact with a disc (representing the valve seat on top); which is preloaded by a compressed linear spring. This concept is represented in Figure 1. The effects on the bell-housing and any other parts such as the nozzle ring are not of interest as it is assumed they do not have any effect on the structural behaviour of the seal.
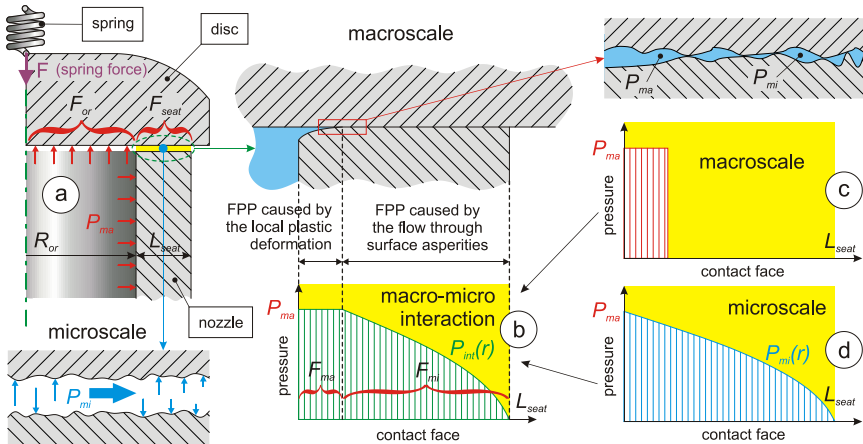

Figure 1: Concept of seat contact configuration in the contact area of metal-to-metal seal considering FPP (fluid pressure penetration).

The compression force of the spring is transferred directly to the disc and then to the seat due to the contact. It is this compression force and quality of the contact which maintains the seal up to the set pressure. For this analysis it is assumed that the contact is geometrically uniform. From the study by Gorash et al. [5], it has been shown that due to FPP the internal contact between the disc and seat significantly deforms due to plastic deformation even at room temperature. The pressure that the FPP attributes to the disc and seat in the contact zone will be known henceforth in this report as the macroscopic pressure distribution.

In reality the contact between the faces of the seat and disc are not uniform, especially at a micro scale, where surface form, waviness and roughness contribute to the leakage. In this case it will be assumed that there is a degree of surface roughness between the contacting faces. To account for this the fluid pressure attributed to surface roughness of the contacting faces in the gap, Müller and Nau [6] had shown that the pressure drop across a sealed gap for a compressed fluid can be represented using a power-law function dependent on distance as:

$$p(x) = P_1\left[1 - \left((1 - \beta^2)\frac{x}{L}\right)\right]^n, \tag{1}$$

where L is a length of a seal gap; P_1 – internal pressure and P_2 – external pressure; so the pressure ratio is $\beta = P_2/P_1$ and $n = 0.5$ a gas. Henceforth in this report this pressure distribution will be related to as the microscopic pressure distribution.

Equation (1) can be extended further by slightly changing the mathematical representation to be aligned with the contact gap in question as explained in Appendix 1:

$$P(r) = P\left[\frac{r_{out} - r}{r_{out} - r_{FPP}}\right]^n. \tag{2}$$

where P – internal pressure, r_{out} – outer radius of the contact area, r – inner radius of the contact area, r_{FPP} – radius of FPP. This micro pressure distribution is formulated in this manner to account for the maximum FPP point travelled in the contact zone.

Integrating Eq. (2) by r over the length of the valve seat ($L_{seat} = r_{out} - r_{in}$), an average value of the pressure within the micro pressure distribution is obtained in analytical form (please refer to Appendix 2 for mathematical manipulation):

$$\bar{P} = \frac{P}{1 + n}. \tag{3}$$

Therefore, the force required by the spring to maintain the required set pressure between the seat and disc is an accumulation of the operating pressure up to the internal office, macro and micro pressure distribution multiplied by the associated areas. Hence the spring force can be represented in the following form:

$$F_{spring} = F_{ORF} + F_{MACRO} + F_{MICRO}, \tag{4}$$

$$F_{spring} = P\pi r_{in}^2 + P\pi\left(r_{FPP}^2 - r_{in}^2\right) + P\pi\left(\frac{1}{1 + n_{POW}}\right) \cdot (r_{out}^2 - r_{FPP}^2). \tag{5}$$

If $n_{POW} = 0.5$ for a gas then

$$F_{spring} = P\pi\left(\frac{2}{3}r_{out}^2 + \frac{1}{3}r_{FPP}^2\right). \tag{6}$$

Alternatively this can be expressed in terms of spring displacement Δ_{sp}:

$$\Delta_{sp} = \frac{P\pi}{K}\left(\frac{2}{3}r_{out}^2 + \frac{1}{3}r_{FPP}^2\right). \tag{7}$$

3   FEA MODELLING AND APDL SCRIPT

The numerical study is conducted using academic FE-code ANSYS 16.0. The three components, cylindrical nozzle, disc and spring are all simplified into a 2D axisymmetric, elastic-plastic model, as shown in Figure 2. The model is set-up as a quasi-static structural analysis allowing the valve to open and close over 100 cycles.

As shown below, the spring is modelled using a COMBIN14 (2-node longitudinal linear spring-damper) Finite Elements (FE). A vertical displacement of Δ_{sp} is applied to compress the spring. As previously described the displacement of Δ_{sp} is proportional to the sealing set pressure, which as elaborated is due to the internal pressure and the macro-micro pressure distribution within the contact area. The spring is connected to the kinematic coupled nodes at the top of the disc. This is to ensure that the vertical force associated with the spring is distributed evenly and vertically down the disc.

The disc and seat are both constructed of PLANE183 (8-node axisymmetric structural solid) FE with an internal pressure, P, placed on the inside and a fixed boundary constraint placed on the outside near the bottom of the seat (i.e. the connection to the outer valve body). The pressure, P, is ramped up with an average pressure change rate of
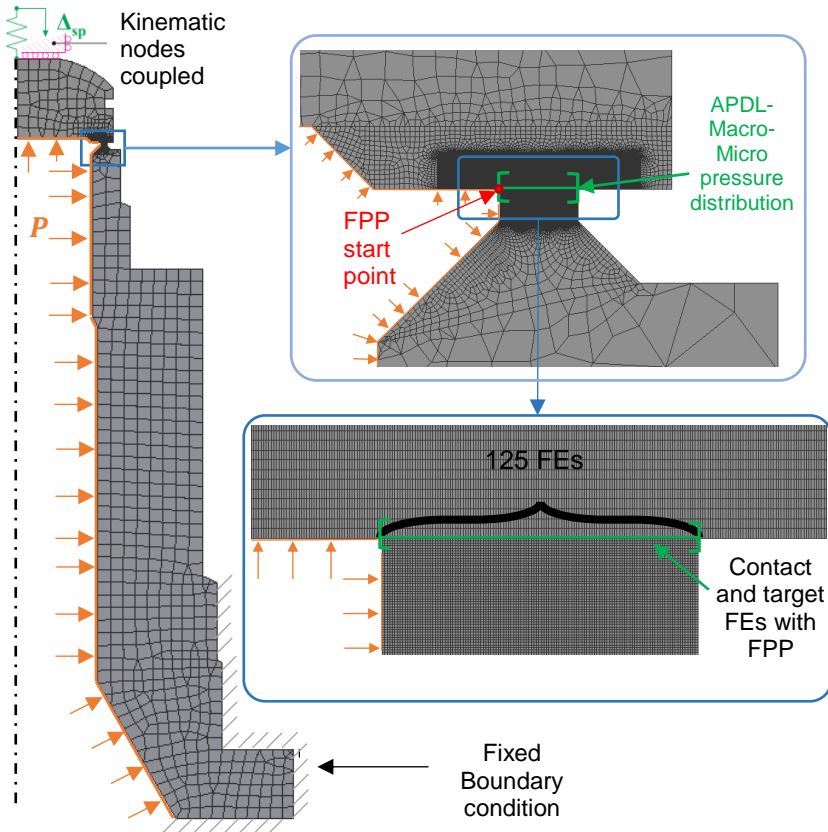

Figure 2: FE model of the valve seat and disc, with a detailed model of the contact zone, boundary conditions and loadings.

$r_{pr} = 0.744$ MPa/s in an incremental manner until the set pressure of 18.6 MPa is reached and then incrementally reduced to zero. This accounts for 1 cycle of the valve opening and closing.

The contact pair is made up of CONTA172 (2D 3-node surf-surf contact {for disk}) and TARG169 (2D 3-node target {seat}). The internal contact of the seat and disc is the associated starting point for the FPP feature and is allowed to penetrate along the full contact length. This FPP feature allows pressure to be associated with changing contact conditions i.e. as the seat and disc deforms a gap is created and it will have the associated pressure applied in it automatically. As the valve ramps up in pressure and cycles open and close, it is expected for the FPP to migrate along the contact length. To account for the micro pressure distribution with respect to the FPP migration point an APDL script is required, so that the macro and micro pressure is applied correctly.

To ensure the FPP is captured accurately a high resolution of contact points are created between the seat and disc (125 FEs in the contact region). In total there are 16404 elements and 49939 nodes. For further information specific to element types please refer to ANSYS® Help (2015) [7].

4   APDL SCRIPT – r_{FPP} RETREIVAL and APPLY

As the pressure incrementally increases, the FPP through the contact between the disc and seat increases gradually until the pressure is either not high enough to penetrate further or the deformation of the seat/disc reduces not allowing further penetration. The location point of the r_{FPP} is important to allow accurate micro pressure distribution to be applied and hence an accurate spring displacement Δ_{sp}. To capture this migration of the r_{FPP} location across the seat and disc an APDL script is required as shown in Figure 3.

Figure 3 is a flowchart of the script which activates after the first Load Step (LS) has solved. The script retrieves the FFP contact data produced from the previous LS from the post processor. It then sorts the data out to find the maximum FPP location across the seat and disc. This data point is saved as r_{FPP} and the script instructs the ANSYS
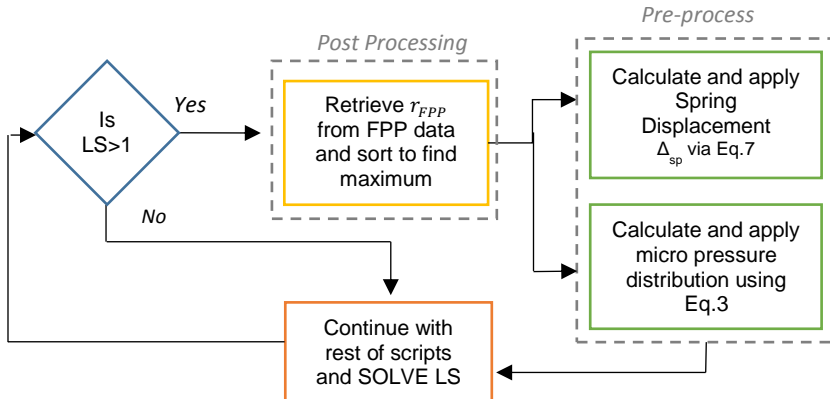

Figure 3: APDL script flowchart – r_{FPP} retrieval, micro pressure application and spring force adjustment.

program to enter the pre-process (/SOLU) state and adjust the spring displacement and micro pressure distribution using Eq. (7) and Eq. (3) respectively. The micro pressure distribution is also applied only across location r_{FPP} to r_{out}.

Once the Post Process and Pre-process stage is complete the program continues with any other scripts and solves for that LS. This process is restarted at the beginning of the next LS until all the LS's are solved.

5   MATERIAL MODEL

The critical components of the PRV (nozzle and disk) are manufactured of the steel AISI type 316N(L) due to optimally appropriate mechanical properties of this steel grade. AISI type 316N(L) stainless steel has been used within the power-generating industry since the early 60s of 20th century. Commonly used in superheater piping, pressure vessels, heat exchangers and other components exposed to high temperatures of 650°C as indicated in previous work [5]. The mechanical characteristics of the steel AISI type 316N(L) makes it an optimal material for a valve seat which is expected to undergo high local contact stresses, corrosion-fatigue conditions and possible high-temperature exposure.

Mechanical properties of the steel AISI type 316 in the range of 20-700°C show significant temperature dependence [8]. Available stress-stain experimental data and its fitting by elastic-perfectly-plastic (EPP) and Ramberg-Osgood (R-O) material models were discussed by Gorash et al. [5]. Compared to martensitic and ferritic steels, austenitic grades including type 316 have lower yield stress σ_y, but higher rupture ductility. This complies with experimental observations at room and high temperatures, which confirm that the material behaviour of the steel AISI type 316N(L) is viscous and rate-dependent [9]. Thus, an accurate description of the plastic deformations with the Chaboche unified viscoplasticity model is essential to address structural integrity and operation issues.

In previous study [5], originally viscoplastic material behaviour of the steel AISI type 316N(L) was simplified to rate-independent plasticity neglecting viscous effects. Available monotonic and cyclic stress-strain curves were fitted by the R-O equation and incorporated through the multilinear kinematic hardening (MLKH) model in ANSYS. Since the dynamic effects have been neglected, the PRV operation was assumed to be quasi-static for FE-simulation in ANSYS.

Consideration of viscoplastic effects for FEA in current work requires the mechanical material properties and Chaboche material constants at a temperature of 538°C. These values are derived by simple interpolation using the experimental data by Hyde et al. [9] available for 300, 500, 550 and 600°C. In order to obtain constants for $T_i = 538$°C, the constants at lower $T_l = 500$°C and upper $T_u = 550$°C neighbouring temperatures are used. The interpolation is done by using the weighting coefficients (lower and upper), which define the proximity of the interpolated temperature to the neighbouring temperatures:

$$w_l = \frac{T_u - T_i}{T_u - T_l} \quad \text{and} \quad w_u = \frac{T_i - T_l}{T_u - T_l}. \tag{8}$$

In this case, the weighting coefficients take the values of $w_l = 0.24$ and $w_u = 0.76$. In general, the following condition should be satisfied for the temperature:

$$T_i = T_l \cdot w_l + T_u \cdot w_u. \tag{9}$$

Equation (9) is used to identify all the material constants for AISI type 316N(L) steel at 538°C using the constants at 500°C and 550°C [9], which are reported in Table 1 and required for implementation of FEA in ANSYS.

Table 1: Material constants for Chaboche model for AISI type 316N(L) steel at 538°C interpolated from constants at 500°C and 550°C [9] using Eqs (8) and (9).

T (°C)	k (MPa)	E (GPa)	b	Q (MPa)	a_1 (MPa)	C_1	a_2 (MPa)	C_2	Z (MPa·s$^{1/n}$)	n
500	32.5	145.54	33.35	30.41	94.6	6472.6	113.3	979.91	175	10
538	*31.36*	*142.29*	*31.56*	*28.43*	*88.29*	*6827.06*	*114.44*	*963.02*	*173.48*	*10*
550	31	141.26	31	27.8	86.3	6939	114.8	957.69	173	10

In order to conclude about the influence of high temperature on cyclic deformation of the valve seal, the material constants for Chaboche model are also required for 20°C. Since the experimental stress-strain curves are available only for a single strain rate value, the rate-independent variant of Chaboche model is used. The identification of corresponding constants is done using the fitting procedure suggested in previous work [10]. This procedure comprises the initial smoothing of the cyclic stress-strain data by the R-O model and subsequent estimation of the kinematic constants using the Solver add-in of Microsoft Excel. The smoothed cyclic stress-strain data is fitted by the following equation [11] for stress amplitude ($\Delta\sigma/2$) and plastic strain amplitude ($\varepsilon^{\mathrm{p}}/2$):

$$\frac{\Delta\sigma}{2} = \sum_i \frac{C_i}{\gamma_i} \tanh\left(\gamma_i \frac{\varepsilon^{\mathrm{p}}}{2}\right). \tag{10}$$

The number of kinematic back-stresses is increased to five ($i = 5$) in order to incorporate the mixed softening-hardening character of plastic deformation observed during cyclic response. The corresponding values of the kinematic constants (a_1- a_5 and C_1- C_5) for the Chaboche model are reported in Table 2. The next step is the identification of isotropic constants (k, b, Q) for the Chaboche model (see Table 2) through fitting of monotonic stress-strain data by the following equation [11] for stress σ and plastic strain ε^{p}:

$$\sigma = k + Q\left[1 - \exp(-b\varepsilon^{\mathrm{p}})\right] + \sum_i \frac{C_i}{\gamma_i}\left[1 - \exp(-\gamma_i \varepsilon^{\mathrm{p}})\right]. \tag{11}$$

Table 2: Material constants for Chaboche model for AISI type 316N(L) steel at 20°C identified using the experimental stress-strain curves and R-O fittings [5].

k (MPa)	E (GPa)	b	Q (MPa)
119.1	194	558.3	-119.1

a_1 (MPa)	C_1	a_2 (MPa)	C_2	a_3 (MPa)	C_3	a_4 (MPa)	C_4	a_5 (MPa)	C_5
454.4	60.6	134.6	899.1	54.5	14289	20	267800	10.5	6729430

6   RESULTS AND DISUCCION

For both the 20°C and 538°C cyclic opening and closing analysis, it is shown that the F_{spring} is required to increase to maintain the desired set pressure as shown in Figure 4. The percentage increase shown in Figure 4 is calculated by:

$$\% \ increase \ of \ F_{spring} = \frac{F_{spring} \ from \ ANSYS}{F_{ORF}} \cdot 100 \qquad (12)$$

For the 20°C the % increase is shown to be 7.48%. This is to account for the initial plastic deformation of the internal contact area of the seat and disc. A further plastic deformation is calculated in the second cycle which shows an increase to 7.5% which it maintains for the rest of the 100 cycles.

The 538°C simulation shows roughly a 1.5 point higher set force than at 20°C at 8.88%. This is maintained for the first 3 cycles which slightly increases at the 4th to 8.93%. There is a sharp increase to 9.45% after which there is an oscillation between 9.3% and 9.45%. This oscillation lasts until the 15th cycle after which a 9.4% increase in F_{spring} is maintained for the rest of the 100 cycles.

This transition between 8.88% and 9.45% can be explained by analysing the plastic deformation across the contacting seat face (Figure 5). The whole of the seat face becomes plastically strained with concentration zones at the internal and external edge (with the former being more significant). Of course the graph is only associated with the seat face. The extent of the plastic zone across the seat is shown in Figure 6 with the two concentration zones being visible again. As can be seen from Figure 6, the disc remains elastic and does not undergo any plastic strain. As the cycles increase the plastic strain on the internal and external edges does increase significantly; 0.1% (1st cycle) – 0.38% (100th cycle) and 0.03% (1st cycle) – 0.25% (100th cycle). The internal plastic zone is most prevalent from 0- 0.5mm while the external edge is 1.08mm-1.25mm. Since this was an idealized model it is clear that the edges no longer remain square and do deform into radial edges, with a small mound shaped middle section (0.4mm-1mm).
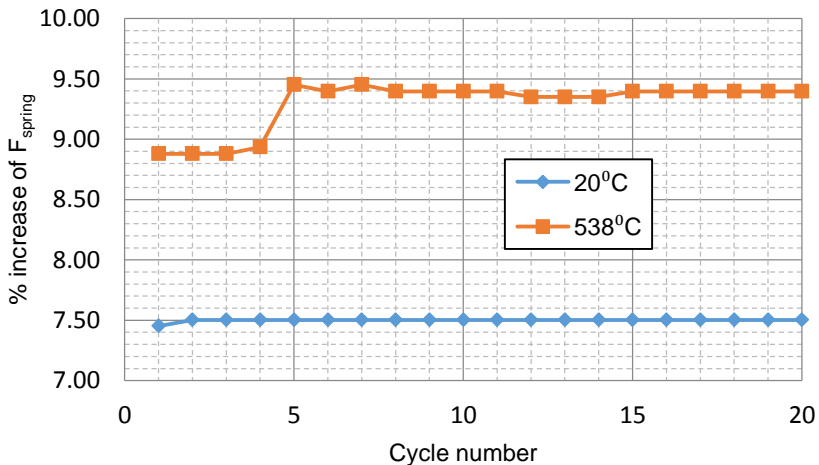

Figure 4: Spring force (%) increase to account for plastic strain development across contacting faces.
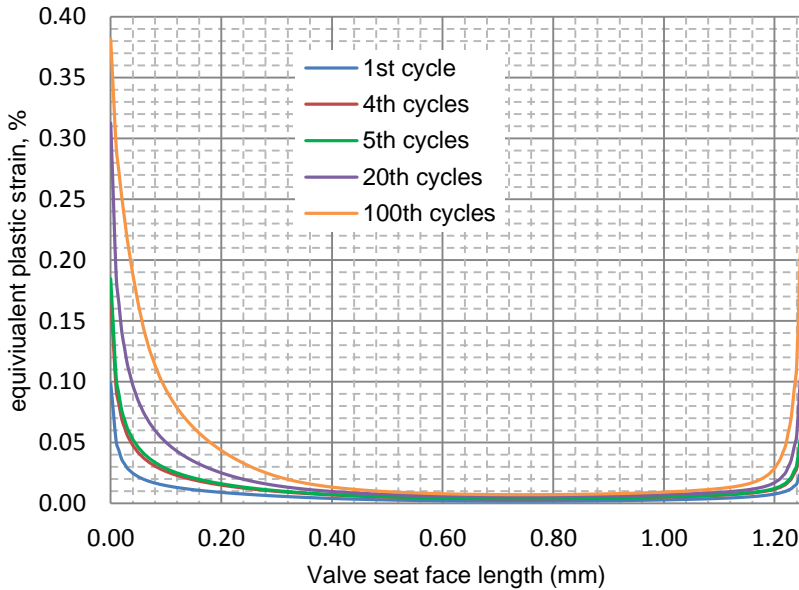
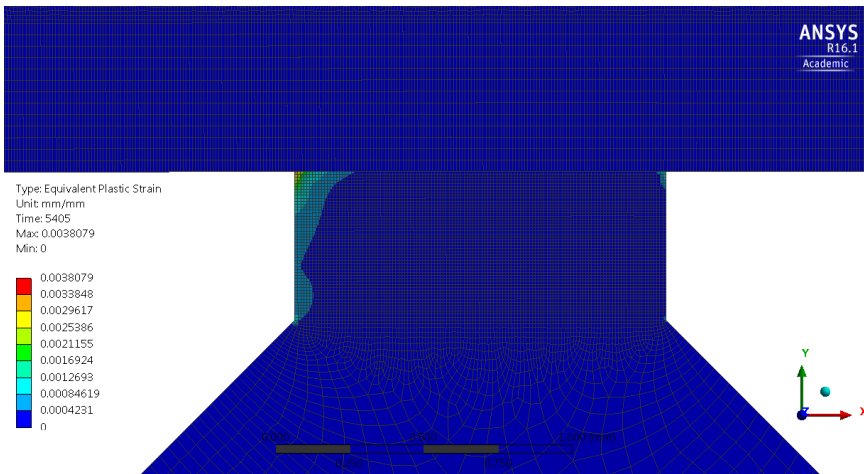**Figure 5: Plastic Strain (%) across seat length (mm)**

Figure 6: Plastic Strain of seat and disc at 100 cycles

The significant internal plastic zone is due to a combination of the Spring Force, FPP and internal pressure, with the former two being the main contributors. As the plastic deformation of the contact face increases the FPP is allowed to migrate further into the contact zone. This requires an increase in the spring force to maintain the required set pressure.

7   CONCLUSION

Using FE-code ANSYS 16.1, it has been shown that to maintain a required set pressure of 18.6 MPa for a gas at a temperature of 538ºC, the spring force must be increased between 8.88% and 9.45%. This has been found to be adequate for up to 100 cycles of the valve opening and closing.

This increase in spring force is found to be due to the lower yield stress and plastic strain conditions of Stainless Steel 316N(L) at 538ºC, combined with FPP and the micro pressure distribution representing the surface roughness. This idealized model did show a significant amount of plastic strain at the internal edge of the seat extending from 0 to 0.5mm in length.

Future research should focus on multiscale approaches and understanding the effects of surface form and waviness as well.

APPENDIX 1

Mathematical manipulation to achieve Eq. (2):

Assuming gauge pressure, $P_2 = 0$, therefore Eq. 1 becomes

$$P(x) = P\left(1 - (1-0)\frac{x}{L}\right)^n = P\left(1 - \frac{x}{L}\right)^n = P\left(\frac{L-x}{L}\right)^n \tag{13}$$

Assuming $L_{seat} = r_{out} - r_{in}$ and x is the distance along the seat length in question, therefore;

$$P(x) = P\left(\frac{r_{out} - (r_{in} + x)}{r_{out} - r_{in}}\right)^n \tag{14}$$

In this case, for the microscopic region only, $r_{in} = r_{FPP}$ and $r = r_{in} + x$, $(r \geq r_{FPP})$ therefore;

$$P(x) = P\left(\frac{r_{out} - r}{r_{out} - r_{FPP}}\right)^n \tag{15}$$

APPENDIX 2

Mathematical manipulation to achieve Eq. (3):

Using the average value of a function [12]:

$$f_{avg} = \frac{1}{b-a} \int_a^b f(x)\,dx \tag{16}$$

Eq. (2) can be integrated using the above equation, with the length of the seat, $L_{SEAT} = r_{out} - r_{in}$, used as limits b and a respectively,

$$\overline{P} = \frac{1}{r_{out} - r_{in}} \int_{r_{in}}^{r_{out}} P \left(\frac{r_{out} - r}{r_{out} - r_{in}} \right)^n dx \qquad (17)$$

$$\overline{P} = \frac{P}{\left(r_{out} - r_{in} \right).\left(r_{out} - r_{in} \right)^n} \int_{r_{in}}^{r_{out}} \left(r_{out} - r \right)^n dx \qquad (18)$$

$$\overline{P} = \frac{P}{\left(r_{out} - r_{in} \right).\left(r_{out} - r_{in} \right)^n}.\left[-\frac{\left(r_{out} - r \right)^{n+1}}{n+1} \right]_{r_{in}}^{r_{out}} \qquad (19)$$

$$\overline{P} = \frac{P}{\left(r_{out} - r_{in} \right)^{n+1}}.\left[0 + \frac{\left(r_{out} - r_{in} \right)^{n+1}}{n+1} \right] \qquad (20)$$

$$\overline{P} = \frac{P}{n+1} \qquad (21)$$

REFRENCES

1. British Standard 6759-3, *Part 3: Specification for safety valves for process fluids,* British Standards1984, UK.
2. ASME / ANSI PTC 25.3 standard, *Pressure Relief Devices*, ASME, 1994, USA.
3. API Standard 527, *Seat Tightness of Pressure Relief Valves*, 3rd edition, American Petroleum Institute, 1991, USA.
4. Smith E. & Vivian, B.E. (1995) *An Introductory Guide to Valve Selection*. 2nd edition, Mechanical Engineering Publications Limited: Suffolk, UK.
5. Gorash Y., Dempster W., Nicholls W.D. & Hamilton R. (2015) Modelling of metal-to-metal seals in a pressure relief valve using advanced FE-analysis. *WIT Trans. on Engineering Sciences (eds. J.Th.M. de Hosson, M. Hadfield & C.A. Brebbia)*, vol. 91, pp. 247-258.
6. Müller H.K. & Nau B.S. (1998) *Fluid Sealing Technology: Principles and Applications*. Marcel Dekker, Inc., New York, USA.
7. ANSYS® Help (2015) *Mechanical APDL > Element Reference > 7. Element Library > Part I: Element Library.* ANSYS, Inc.: Canonsburg (PA), USA (Academic Research 16.1 ed.).
8. Gorash Y., Altenbach H. & Lvov G. (2012) Modeling of high-temperature inelastic behavior of the austenitic steel AISI type 316 using a continuum damage mechanics approach. *J. Strain Analysis* 47(4), pp. 229 – 243.
9. Hyde C.J., Sun W. & Leen S.B. (2010) Cyclic thermo-mechanical material modelling and testing of 316 stainless steel. *Int. J. of Pressure Vessels & Piping* 87(6), pp. 365-372.
10. Gorash Y. & MacKenzie D. (2014) Safe structural design for fatigue and creep using cyclic yield strength. *Proc. 3rd Int. ECCC Conf. – Creep & Fracture* (May 5-7, 2014, Rome, Italy), paper no. ECCC2014-87, 12 p.
11. Chaboche J.-L. (2008) A review of some plasticity and viscoplasticity constitutive theories. *Int. J. Plasticity* 24(10), pp. 1642-1693.
12. Wikipedia, Mean of a function: https://en.wikipedia.org/wiki/Mean_of_a_function 21 Aug 2014.

ACKNOWLEDGEMENTS